

EMI Filter Design for High Switching Frequency Three-Phase/Level PWM Rectifier Systems

M. Hartmann*, H. Ertl[†] and J. W. Kolar*

* Power Electronic Systems Laboratory, Swiss Federal Institute of Technology Zurich, Switzerland; Email: hartmann@lem.ee.ethz.ch

[†] Institute of Electrical Drives and Machines, Power Electronics Section University of Technology Vienna, Austria; Email: j.ertl@tuwien.ac.at

Abstract—The actual attenuation characteristic of EMI filters in practice often differs from theoretical predictions and minor changes could result in a significant performance improvement. Whereas the performance of the differential-mode (DM) filter stage usually can be well predicted, the common-mode (CM) behavior is more difficult to handle. This is especially true for three-phase PWM rectifier systems, which show a large high-frequency CM voltage at the rectifier output. In this work the possible CM noise current paths of a three-phase/level PWM rectifier are analyzed where parasitic capacitances to the heat sink and to earth are considered. Additionally, a concept to significantly reduce CM emissions is discussed in detail. Based on the proposed models an EMI filter design for a system with 1 MHz switching frequency is shown. Experimental verification of the designed EMI filter is presented by impedance and conducted emission (CE) measurements taken from a 10 kW hardware prototype. Several practical aspects of filter realization like component arrangement, shielding layers, magnetic coupling etc. are discussed and verified by measurements.

I. INTRODUCTION

For new application fields (e.g. power electronics in aircraft [1]) modern rectifier systems have to meet high requirements concerning efficiency, weight and compactness. Active three-phase rectifiers offer the possibility to comply with rigorous low-frequency current harmonics limits but show a large high frequency noise level. Passive low-pass filters employing inductors and capacitors in connection with resistors providing passive damping can be used to attenuate resulting conducted emissions (CE) of the systems [2]-[3]. These passive filter elements take up a relatively large portion of overall system volume and can only be reduced in volume by increasing the switching frequency.

It is common and very helpful to split the generated EMI emissions into a common-mode (CM) and differential-mode (DM) component. Whereas DM noise currents flow in and out through the phases, CM currents return via earth. Hence, different filter strategies and filter elements have to be applied to handle the two emission types. However, as will be shown in section II, asymmetrical currents to earth caused by asymmetrical impedances of the rectifier system also generate DM noise. These type of emissions are called “mixed-mode noise” (MM) and their origin was analyzed in [4]-[5] for single-phase flyback converters. MM noise in three-phase diode front-end converters was discussed in [6]-[7].

The performance of the DM filter can be well predicted. Commonly (dependent on the required attenuation) multi-stage LC-filters are applied [8]. Also “zero-ripple” DM filter concepts have been proposed [9]. On the contrary, CM emissions are mainly determined by parasitic elements like capacitances of semiconductors to the heat sink, capacitances between heat sink and earth, magnetic couplings of inductors etc. and are therefore difficult to identify and quantify.

In this work an EMI filter design and realization for an ultra-compact three-phase/level PWM rectifier (cf., Fig. 1 where

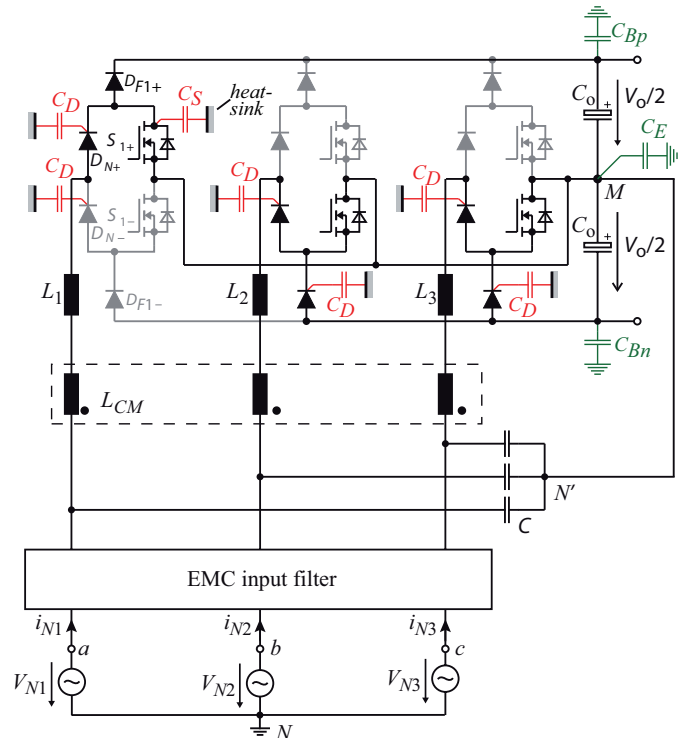


Fig. 1: Schematic of the three-phase/level PWM rectifier including relevant parasitic capacitances from semiconductors to heat sink (C_S , C_D) and from the DC output rails to earth (C_{BP} , C_{BN} and C_E) for $i_{N1} > 0$, $i_{N2}, i_{N3} < 0$. Additionally, the proposed CM voltage reduction concept is shown, where the output voltage midpoint M is connected to an artificial mains star point N' . High frequency CM currents are limited by a three-phase CM inductor L_{CM} .

the parasitic capacitances relevant for $i_{N1} > 0$, $i_{N2}, i_{N3} < 0$ are shown) [10] will be discussed. The realized filter should show minimum volume in order to achieve a highest possible rectifier power density. Accordingly, a switching frequency of 1 MHz is chosen [11].

In [12] the formation of the CM voltage was analyzed in detail but for sake of simplicity only a single lumped capacitor from the output voltage midpoint M to earth was used to model the CM current paths. This is a reasonable approach to get an overview of the CM behavior of a system but turns out to be not sufficiently accurate for designing the EMI filter. Hence, a more detailed CM model considering parasitic capacitances of the semiconductors to the heat sink and from the output voltage rails to earth is developed in section II.

In [12] also a concept for minimizing the high-frequency CM emissions was proposed (further concepts can be found in [13]). There, the output voltage midpoint M is connected to an artificial mains star-point N' formed by capacitors C . Whereas the low-frequency CM voltage used to increase the input voltage range of

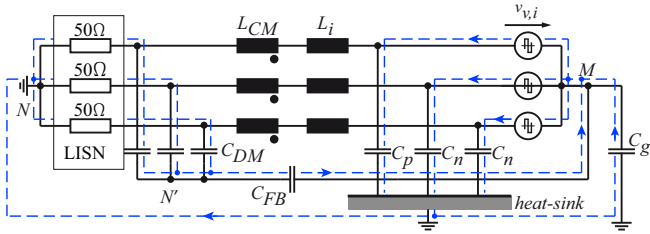


Fig. 2: Detailed noise model valid for $i_{N1} > 0$, $i_{N2}, i_{N3} < 0$ if the heat sink is connected to earth. Only current paths involving the parasitic capacitors C_p and C_n are shown.

the rectifier drops across the capacitors C , the high frequency CM output voltage is attenuated by a low-pass filter action of the boost inductors L_i and the capacitors C . Unfortunately, this concept results in a considerably increased ripple of the boost inductor currents and/or in higher copper and core losses. Therefore, the basic concept is extended here by placing a three-phase CM inductor L_{CM} in series to the boost inductors L_i which considerably reduces the additional high-frequency current ripple.

The DM filter design as well as the design of the proposed CM filter inductor will be discussed in section III where also a simplified method for determining the CM noise level is proposed. Section IV deals with the practical realization of the filter considering available magnetic materials. Measurements taken from a 10kW rectifier prototype verify the effectiveness of the proposed EMI filter in section V. In this section also several practical aspects of filter realization like the physical components arrangement, shielding layers, and magnetic couplings etc. are discussed with reference to measurement results.

II. CONVERTER NOISE MODEL

The semiconductors of a power electronics converter are typically mounted on a common heat sink which usually is connected to earth. Therefore, parasitic capacitances to earth exist which are not included in the basic circuit diagram. In order to fully understand the propagation of the resulting CM noise currents these capacitances have to be considered and/or a detailed CM noise model has to be derived. Accordingly, in the following the modeling approach given in [19]-[20] for single-phase PFC will be extended to three-phase systems.

In **Fig. 1**, the relevant parasitic capacitors between semiconductors and heat sink are drawn for $i_{N1} > 0$, $i_{N2}, i_{N3} < 0$. The capacitors C_S and C_D represent the stray capacitance of a MOSFET's drain and a diode's cathode to the heat sink which is approximately 60 pF for the applied TO220 package. Actually, these capacitances are present for all semiconductors of the rectifier system, but capacitors which are not carrying current in $-30^\circ < \varphi_N < 30^\circ$ are not shown. The capacitors C_{Bp} and C_{Bn} model the stray capacitances of the positive and negative output voltage rail to earth. The capacitor C_E models the parasitic capacitance of the output voltage midpoint to earth but also includes possible parasitic capacitances of the load. Therefore, the capacitance of C_E can be comparably large, i.e. several nF. In order to develop a high-frequency CM model of the circuit the MOSFETs are replaced by voltage sources $v_{v,i}$, which impress the switched voltage waveforms. Similarly, the diodes D_{F1+} , D_{F2-} and D_{F3-} are replaced by current sources showing the same pulsed current waveform. The impedance of the output capacitor C_o is typically very small at switching frequency (1 MHz) and therefore modeled as a short-circuit. As can be verified easily, the current sources do not contribute to the CM noise (cf., [20]). The mains diodes are permanently on during a half mains period and are, hence

replaced by a short-circuit. The resulting three-phase noise model of the rectifier is depicted in **Fig. 2**. The phase leg with positive input current (i_{N1}) shows a total capacitance of $C_p = 2C_D + C_S$ to the heat sink and the phase-legs with negative input currents (i_{N2} and i_{N3}) show a total capacitance of $C_n = 2C_D$ which is different to C_p . Note that this model is only valid for $i_{N1} > 0$, $i_{N2}, i_{N3} < 0$, i.e. $-30^\circ < \varphi_N < 30^\circ$, and that the capacitance of C_p and C_n is changing if one of the input phase currents changes sign, i.e. every 60° . The capacitor C_g models all capacitances from the output voltage rails and the output voltage midpoint to earth ($C_g = C_E + C_{Bp} + C_{Bn}$). The detailed function of the CM filtering based on a connection of M with N' will be discussed later. Note, that the voltage sources $v_{v,i}$ include DM emissions as well as CM emissions.

Now, different possibilities for defining the heat sink potential exist where the most important ones are:

- 1) heat sink connected to earth
- 2) heat sink connected to the output voltage midpoint M
- 3) heat sink floating.

All three connection types result in different CM behavior. If the heat sink is connected to M the noise currents through C_p and C_n are directly guided back to the noise source and thus no additional external CM noise occurs. The largest impact on the noise emissions can be observed if the heat sink is connected to earth and this scenario will be further discussed.

Unfortunately, the three phases show different capacitive couplings to earth and therefore a separation into CM and DM emissions is not directly possible. Due to asymmetry the currents of the phases towards earth also generate DM noise. This noise can be called "mixed-mode noise" (cf., [4]-[7]). For the sake of brevity this is not further analyzed in this work but is subject for further research on this topic.

III. FILTER DESIGN

In order to design a proper EMI filter the CM and DM noise levels of the three-phase rectifier system are required. A computer simulation is used to determine the DM and CM voltage waveforms (cf., **Fig. 3(a)** and **Fig. 3(b)**) generated by the rectifier system. The assumed system specifications are listed in TABLE I. Note, that different modulation strategies result in different CM and DM voltage waveforms which would finally lead to different EMI filter requirements. However, for the sake of brevity this is not further discussed in this paper. In three-phase PWM rectifier systems, a third harmonic signal is added to the sinusoidal phase voltage reference values in order to increase the input voltage modulation range for a given output DC voltage. A triangular shaped signal

$$v_{h3} = \frac{\hat{V}_N}{6} \text{tri}(3\varphi) \quad (1)$$

is employed in the implemented modulator which results in a triangular low-frequency component ($v_{CM,avg}$) of the CM voltage (cf., **Fig. 3(b)**).

According to the calculation scheme given in [8] the quasi-peak (QP) or peak (PK) weighted DM and CM spectrum can be calculated. The calculated spectra (using peak-detection) of the voltages shown in **Fig. 3(a)-(b)** are depicted in **Fig. 3(c)-(d)**, together with the limit defined by CISPR11 class A [14]. Note, that the result of this calculation are only the spectra of the simulated voltage waveforms and that, contrary to [8], the influence of the LISN is not considered. The EMI filter has now to be designed such that the generated emissions do not exceed the

TABLE I: Specifications of the analyzed PWM rectifier system.

V_{Ni}	230 V
f_N	50/60 Hz
f_s	1 MHz
V_o	800 V _{DC}
P_o	10 kW

CISPR11 class A. The influence of the LISN has to be considered later in the EMI filter design process.

According to **Fig. 3**, the main amplitudes of harmonics occur at multiples of the switching frequency. Hence, the required attenuation of the DM and CM filter can be calculated by comparing the simulated emissions with the limit specified in CISPR11. For the DM filter this results in a required attenuation of

$$Att_{DM}[\text{dB}] = v_{DM}(f_s)[\text{dB}\mu\text{V}] - Limit[\text{dB}\mu\text{V}] + margin[\text{dB}] \cong 103 \text{ dB} , \quad (2)$$

where a margin of 6 dB is included. The required attenuation of the CM filter can be calculated to

$$Att_{CM}[\text{dB}] = v_{CM}(f_s)[\text{dB}\mu\text{V}] - Limit[\text{dB}\mu\text{V}] + margin[\text{dB}] \cong 93 \text{ dB} . \quad (3)$$

The employed process for calculating the noise spectra is a time consuming task. The result of this calculation are noise amplitudes over the whole frequency range but as shown before only the amplitude of the emissions generated at the switching frequency fundamental is used for EMI filter design (in case of $f_s \geq 150 \text{ kHz}$). In [15] an approximation method for determining the EMI emission has been presented, where only the fundamental DM component at the switching frequency is considered. However, this method can also be applied to determine the CM filter requirements. Therefore, the rms value of the CM voltage $V_{CM,rms}$ which comprises a low-frequency component $V_{CM,h3,rms}$ and a high-frequency component $V_{CM,noise,rms}$ containing all switching frequency harmonics has to be calculated. This could be done purely analytically but for sake of simplicity the rms value of the total CM voltage is calculated using the simulated CM voltage shown in **Fig. 3(b)**. The rms value of the high-frequency CM noise $V_{CM,noise,rms}$ is therefore given by

$$V_{CM,noise,rms}^2 = V_{CM,rms}^2 - V_{CM,h3,rms}^2 . \quad (4)$$

Substituting (1) in (4) yields

$$V_{CM,noise,rms}^2 = V_{CM,rms}^2 - \frac{\left(\frac{\hat{V}_N}{6}\right)^2}{3} \quad (5)$$

which results in an estimated noise level of

$$V_{CM,noise} = 164 \text{ dB}\mu\text{V} . \quad (6)$$

The difference to the result given in **Fig. 3(d)** is only 4 dB μV and therefore, the proposed procedure is a very simple method to estimate the EMI filter requirements.

According to **Fig. 3(c-d)** a relatively large noise floor of $\approx 110 \text{ dB}$ is generated by the rectifier system. The reason for this can be found in the time behavior of the DM and CM voltages. As reported in [16] and [17] carrier sideband harmonics are present in the spectrum of a PWM signal with low-frequency local average. This leads to an increased noise floor which has to be considered in the DM filter design. Therefore, the DM filter has to realize an attenuation of at least

$$Att_{DM2}[\text{dB}] = v_{DM}(150 \text{ kHz})[\text{dB}\mu\text{V}] - Limit[\text{dB}\mu\text{V}] + margin[\text{dB}] \cong 37 \text{ dB} \quad (7)$$

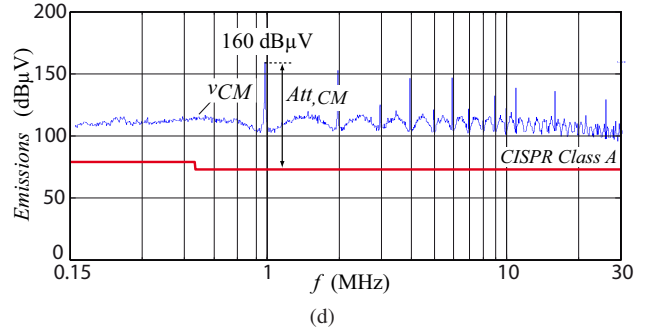
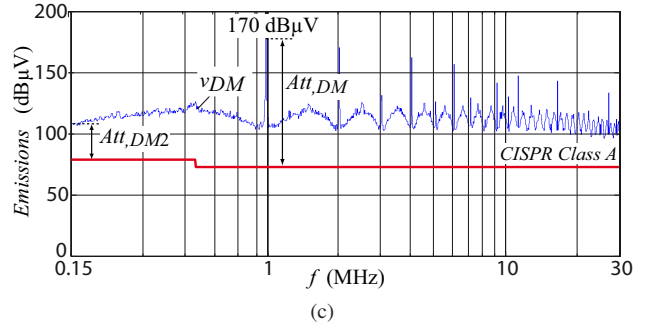
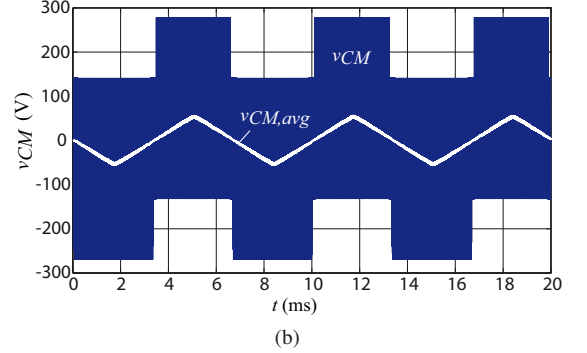
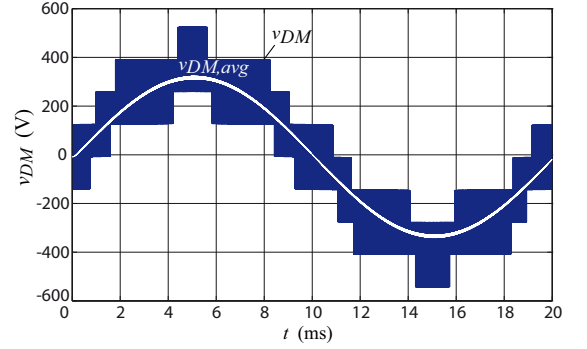


Fig. 3: Simulated voltage waveforms of the rectifier system operated at an output power of $P_o = 10 \text{ kW}$ and corresponding predicted spectra using peak-detection; a) DM voltage; (b) CM voltage; (c) Predicted DM emission and (d) predicted CM emission.

at the lower frequency limit for conducted emissions measurements, i.e. at 150 kHz. Accordingly, at least one filter stage has to be designed such that the required attenuation at 150 kHz is realized, that means the volume of this filter stage can not be reduced by a high switching frequency. Among other limitations like the lack of available high frequency magnetic materials this is a main limitation of EMI filter volume reduction by increasing the switching frequency.

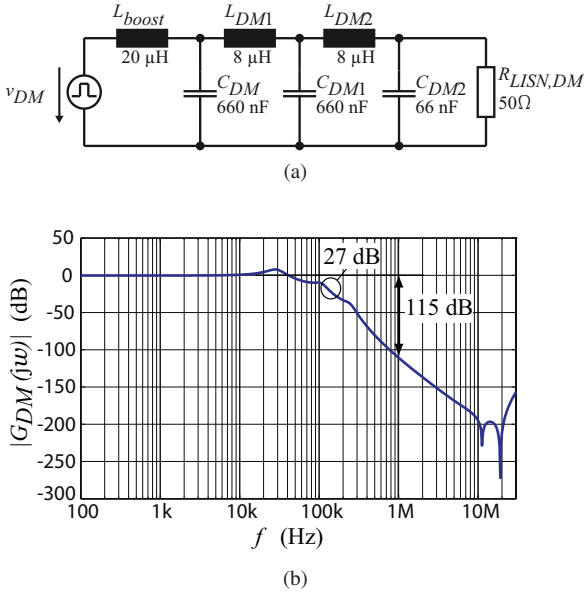


Fig. 4: (a) Equivalent single-phase DM model and (b) calculated transfer function $G_{DM}(j\omega)$ of the designed DM filter.

A. DM Filter Design

For DM filter design, in addition to the required filter attenuation also the phase displacement of the mains currents resulting from the currents drawn by the filter capacitors has to be considered. If a maximum phase displacement should be limited to 10° at an output power of $0.1P_o$, the DM filter capacitors are limited to a total capacitance of $C_{DM} = 3.5 \mu\text{F}$ per phase. According to the specifications given in (2) and (7) an LC-filter with three stages is used for realization of the DM filter. The single-phase equivalent circuit of the DM filter is shown in Fig. 4(a). The boost inductor of the rectifier can be used to realize the first filter stage. The inductance value of the boost inductor is defined by the maximum allowed current ripple. For the realization at hand a maximum current ripple of $\Delta i_{L,pp} = 0.2 \hat{I}_{N,i}$ shall be allowed which results in an inductance of $L_i = 20 \mu\text{H}$. In [18] it was shown that a maximum attenuation for a multi-stage LC-filter can be achieved if all inductance values and all capacitance values are equal, which also implies that the cut-off frequencies of all filter stages are identical. Unfortunately, (2) as well as (7) have to be satisfied which is not possible with regard to a minimum filter volume by application of this criteria. Additionally, this concept shows the problem of multiple equal filter resonance frequencies. Hence, the cut-off frequencies of the filter stages are selected in a distributed manner and the resulting filter components are chosen also considering aspects of practical realization, which will be further discussed in section IV. The calculated transfer function $G_{DM}(j\omega)$ of the designed filter is depicted in Fig. 4(b).

B. CM Filter Design

For a first step design of the CM filter the influence of the parasitic capacitors C_p and C_n (cf., Fig. 2) is neglected. For selecting the CM capacitors safety regulations have to be considered where the leakage earth current is limited to several mA. This results in a limited total capacitance connected to earth which fundamentally influences CM filter design. If a conventional multistage LC low-pass filter would be realized at least three stages would be necessary. Furthermore, the large CM component of V_o would still be present. However, by connecting the output-voltage midpoint M to an artificial star-point N' as shown in Fig. 1, the CM component of the output voltage can be reduced significantly without violating the safety regulations. For the

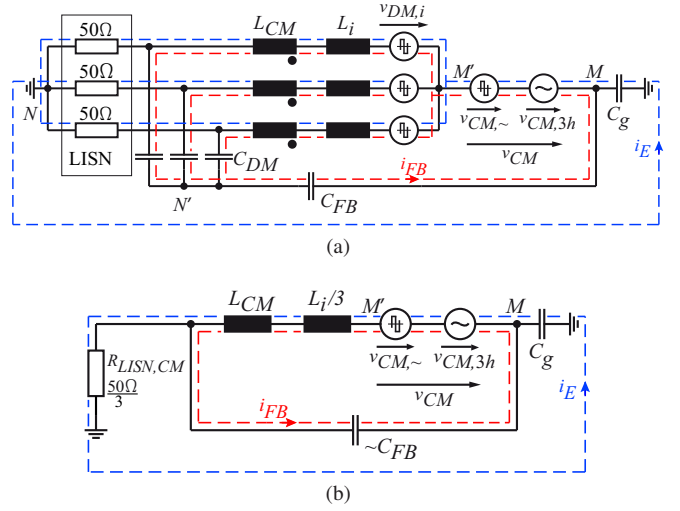


Fig. 5: (a) Conducted noise equivalent circuit of the three-phase/level PWM rectifier system for the proposed CM filter concept if C_p and C_n are neglected; (b) simplified CM equivalent circuit.

formation of N' the capacitors C_{DM} of the first DM filter stage can be used advantageously. An equivalent circuit of the proposed CM filter concept is shown in Fig. 5(a). There, the converter voltage $v_{v,i}$ is split into a DM voltage $v_{DM,i}$ and a CM voltage v_{CM}

$$v_{v,i} = v_{DM,i} + v_{CM} \quad (8)$$

where the CM voltage

$$v_{CM} = v_{CM,\sim} + v_{CM,3h} \quad (9)$$

comprises a high-frequency component $v_{CM,\sim}$ and a low-frequency component $v_{CM,3h}$ which represents the mentioned third harmonic injection. The CM filter path is realized with a capacitor C_{FB} in series to the DM capacitors forming N' . Additionally, the capacitance C_g is shown which represents the lumped capacitance between M and earth which is significantly influenced by the load. If this parasitic capacitance is neglected for a first analysis, the generated CM voltage appears across circuit L_i , L_{CM} and the series connection of the capacitors C_{FB} and C_{DM} . The capacitors C_{FB} and C_{DM} are not connected to earth and are therefore not limited in capacitance by equipment safety regulations. The realization of a CM inductor which is able to handle the third harmonic voltage component $v_{CM,3h}$ without saturation is possible but would result in a very large and bulky element. If the feedback capacitor C_{FB} is dimensioned such that it represents a short-circuit for the high-frequency CM signals ($v_{CM,\sim}$) but a high impedance element for the third harmonic component ($v_{CM,3h}$), the low-frequency component will drop across the feedback capacitor and only $v_{CM,\sim}$ has to be handled by the inductors. Unfortunately, three-phase CM inductors typically allow only a very small zero-sequence current without saturation because of their very high permeability. Because of

$$i_{FB,3h} \approx C \frac{dv_{CM,3h}}{dt} \quad (10)$$

the feedback capacitor has to be as small as possible to prevent saturation of the CM inductor. Hence, the relatively large DM capacitors C_{DM} (660 nF per phase) solely can not be used for realization and a low capacitance feedback capacitor C_{FB} is connected in series to the star-point N' .

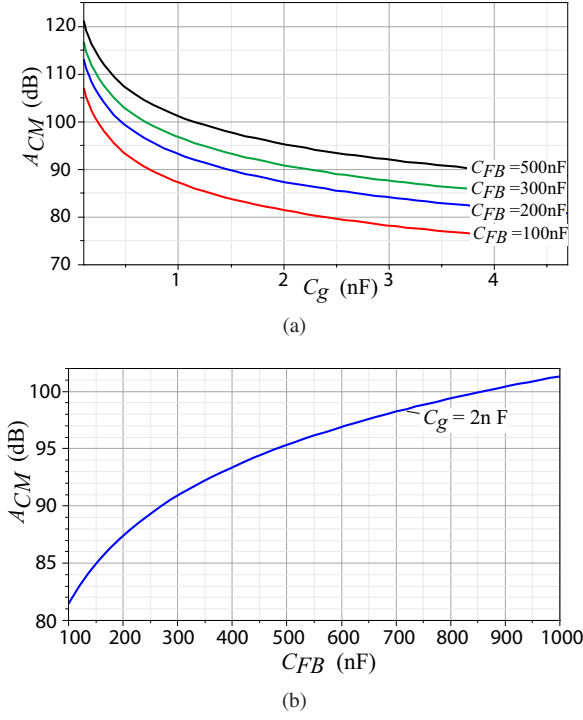


Fig. 6: (a) Attenuation A_{CM} of the proposed CM filter concept as a function of earth capacitance C_g and (b) achieved attenuation as a function of C_{FB} for $C_g = 2\text{ nF}$ ($f = 1\text{ MHz}$).

The CM inductor on the other hand has to hold the high-frequency CM voltage and core saturation is avoided if

$$B_{sat} > B_{CM,max} = \frac{\int_0^{T_p} v_{CM,\sim} dt}{N A f_e} = \frac{V_o T_s}{N A f_e} \quad (11)$$

where $T_s = 1/f_s$ and T_p denotes the maximal length of a CM pulse which was set to $T_p = T_s$.

Since the CM inductors are placed in series to the boost inductors L_i the full phase current including the high-frequency ripple flows through their windings. The high-frequency DM current ripple does not cause core losses because of the mutual compensation of the magnetomotive forces but copper losses caused by skin and proximity effect have to be considered.

In **Fig. 5(b)** the CM equivalent circuit is shown. If the lumped capacitance C_g is not neglected, part of the total CM current doesn't return through the feedback path i_{FB} . Depending on the size of C_g this results in a notable earth current through the line impedance stabilization network (LISN). In order to limit this current the feedback capacitor should be large which, however, is in discrepancy with the design criteria given in (10). Depending on the parasitic capacitances C_g and C_{FB} the attenuation A_{CM} can be calculated by

$$A_{CM} = 20 \log_{10} \left(\left| \frac{1 + A s + \underline{Z}_L C_g C_{FB} R_{LISN,CM} s^2}{R_{LISN,CM} C_g s} \right| \right)$$

$$A = C_g (\underline{Z}_L + R_{LISN,CM}) + \underline{Z}_L C_{FB} \quad (12)$$

where \underline{Z}_L denotes the total impedance of the CM inductor and $R_{LISN,CM}$ is the equivalent high-frequency CM LISN impedance ($R_{LISN,CM} = 16.7\ \Omega$). In **Fig. 6(a)** the resulting attenuation of the realized filter is plotted as a function of the earth capacitance C_g . It is obvious that the required attenuation of 93 dB can only be realized with the proposed concept if either $C_{FB} > 500\text{ nF}$ or $C_g < 1\text{ nF}$. A higher amount of capacitance to earth would result in an attenuation lower than the required

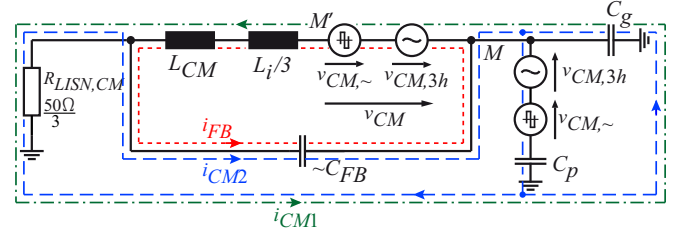


Fig. 7: CM equivalent circuit of the three-phase/level PWM rectifier with heat sink connected to earth if C_p and C_n are assumed to be equal.

value given in (3). According to **Fig. 6(b)**, a higher capacitance of C_{FB} would increase the attenuation but this would also increase the low-frequency current $i_{CM,h3}$ and is therefore no option. For the realization presented in this paper a compromise of $C_{FB} = 200\text{ nF}$ is used. Hence, an additional CM filter stage is required which has to realize the missing attenuation of $\approx 20\text{ dB}$.

Up to this point, the capacitors C_p and C_n of the extended noise model given in **Fig. 2** have been neglected for CM filter design. According to (8) the total converter noise $v_{v,i}$ can be divided into DM and CM emissions, if the two lumped parasitic capacitors are assumed to be equal ($C_p = C_n$). Hence, a simplified CM model can be drawn which is shown in **Fig. 7**. It is obvious, that even if the proposed CM concept operates ideally ($i_{CM1} = 0$) a CM current i_{CM2} through the LISN exists (marked as blue dashed line). This current is caused by the parasitic capacitances of the semiconductors to the heat sink (if the heat sink is connected to earth) and can only be reduced by insertion of an additional CM filter stage. However, as already discussed, this additional filter stage is needed anyway in order to realize the required attenuation given in (3). It has to be stated here, that the proposed CM filter concept (connection of M with N') supports the propagation of this type of CM emissions and that a large capacitance C_g would help to reduce the emissions. However, the advantage of an output voltage without high-frequency CM component clearly dominates this drawback.

IV. FILTER REALIZATION

After determination of the EMI filter topology and calculation of the filter performance the realization of the passive components is an important design step. Here, a proper magnetic material has to be chosen for realization of the inductors. In **Fig. 8(a)** the complex permeability $\mu = \mu' - j\mu''$ of the widely used ferrite materials N97 and N49 from EPCOS Inc. are plotted. According to **Fig. 8(a)**, the real part of the permeability μ' of material N97 is only constant up to $\approx 1\text{ MHz}$ and drops quickly for higher frequencies. Moreover, also the imaginary part μ'' which is related to core losses rises steeply. Consequently, the magnetic material N97 can not be applied for realizing the boost inductor and is also not a good option for DM filter inductor realization. A realization using material N49 would be possible for $f_s = 1\text{ MHz}$ but unfortunately, no suitable core size is commercially available. The permeability of the powder core-material -8 from Micrometals Inc. stays constant up to 100 MHz (cf., **Fig. 8(b)**) and shows acceptable losses and is therefore used for implementation of the DM and boost inductors. Single layer winding toroids T90-8 with $N = 16$ turns are used for realizing the DM inductors with very small parasitic capacitance. This results in a high self-resonance frequency of 25.9 MHz. For the realization of the DM capacitors C_{DM1} and C_{DM2} three 220 nF/630V X7R ceramic capacitors in parallel are used. Unfortunately, the capacitance of these ceramic capacitors is strongly dependent on the applied voltage which results in a much smaller effective capacitance. Hence, for the

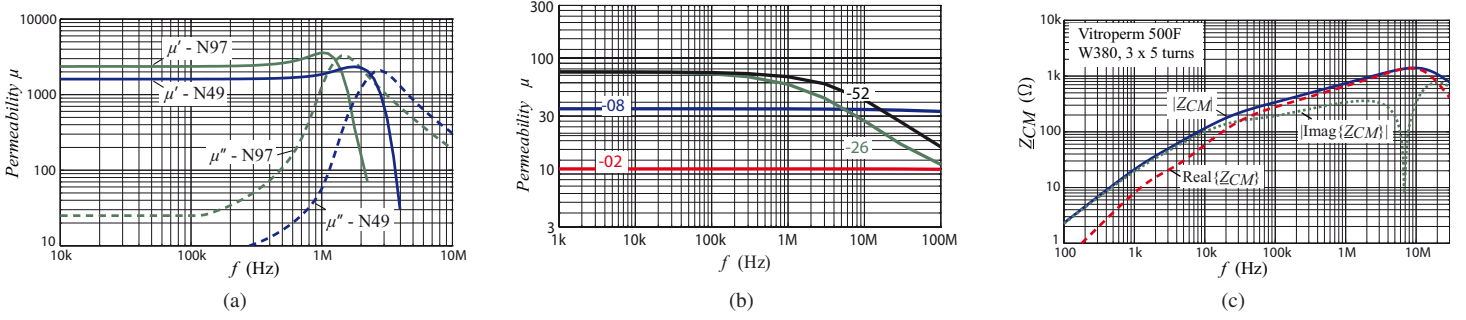


Fig. 8: Real and imaginary part of complex permeability $\mu = \mu' - j\mu''$ for (a) ferrite materials N97 and N49 of EPCOS and (b) initial permeability for powder core materials from Micrometals. (c) Measured impedance of the realized three-phase CM inductor ($N = 5$ turns) employing Vitroperm 500F from VAC.

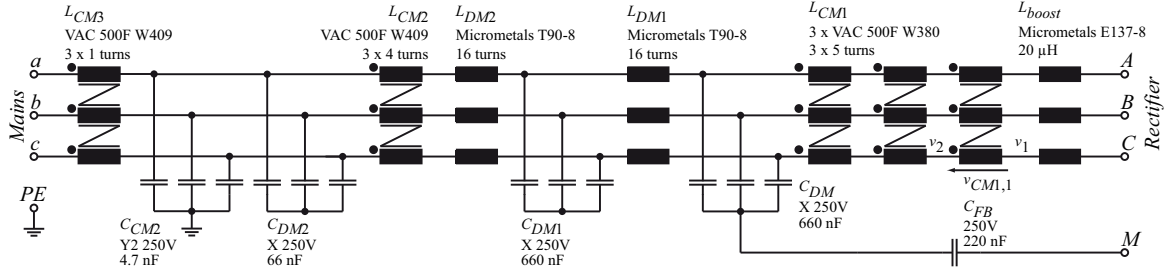


Fig. 9: Complete schematic of the realized EMI filter including information on the used materials.

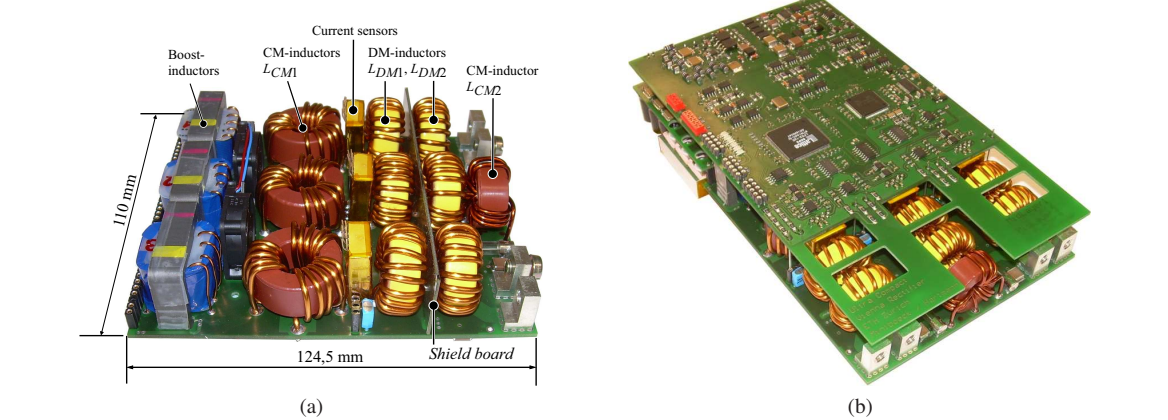


Fig. 10: (a) Realized prototype of EMI filter and (b) 10 kW laboratory prototype of the ultra-compact rectifier system (Dimensions: 195 mm x 110 mm x 33 mm).

realization at hand five capacitors have to be used. This can be avoided by application of foil capacitors resulting however in a larger volume.

For realization of the CM inductors the nanocrystalline material Vitroperm 500F of Vacuumschmelze Inc. is used. The measured complex insertion impedance Z_{CM} of the CM inductor is plotted in **Fig. 8(c)**. It can be seen that the inductor exhibits a substantial real part of Z_{CM} at $f = 1$ MHz which has to be considered for the design of the CM filter stage. Three inductors are connected in series for realization of L_{CM1} in order to limit the core losses. For the second CM filter stage a core W409 (also utilizing Vitroperm 500F) is used in conjunction with 4.7 nF Y2-rated ceramic capacitors which show a very small volume.

The complete schematic of the realized filter including detailed information on the used materials is given in **Fig. 9**. For arrangement of the different filter stages the impedance mismatch concept described in [21] has to be used. According to this concept the impedance of the last DM filter stage (C_{DM2}) should be much smaller than the impedance of the LISN ($R_{LISN,DM} = 50 \Omega$) which is given for the arrangement shown in **Fig. 9**. This should also be considered for the last CM filter stage (C_{CM2}). However,

the LISN shows a reduced CM impedance $R_{LISN,CM} = 16.7 \Omega$ and in addition the impedance reduction of the last CM filter stage is limited by equipment safety regulation (C_{CM2}). Therefore, an additional CM inductor (L_{CM3}) is needed to fulfill the impedance mismatch constraint. This CM inductor is realized with a ferrite core which is clamped on the power cable.

The CM inductors are placed in series to the DM inductors because the stray inductance of the CM inductors then can be used advantageously to increase the DM attenuation. The realized EMI filter prototype is shown in **Fig. 10(a)** together with a picture of the 10 kW laboratory prototype of the rectifier (**Fig. 10(b)**). The overall dimensions of the EMI filter board are 124.5 mm x 110 mm x 33 mm which results in a power density of 22.1 kW/dm³ for the EMI filter. The overall rectifier system with the dimensions 195 mm x 110 mm x 33 mm shows a power density of 14.1 kW/dm³.

V. EXPERIMENTAL RESULTS

In **Fig. 11** the results of an EMI measurement according to CISPR 11 (frequency range 150 kHz...30 MHz) are shown together with the limits of CISPR 11 class A. A three-phase DM/CM noise

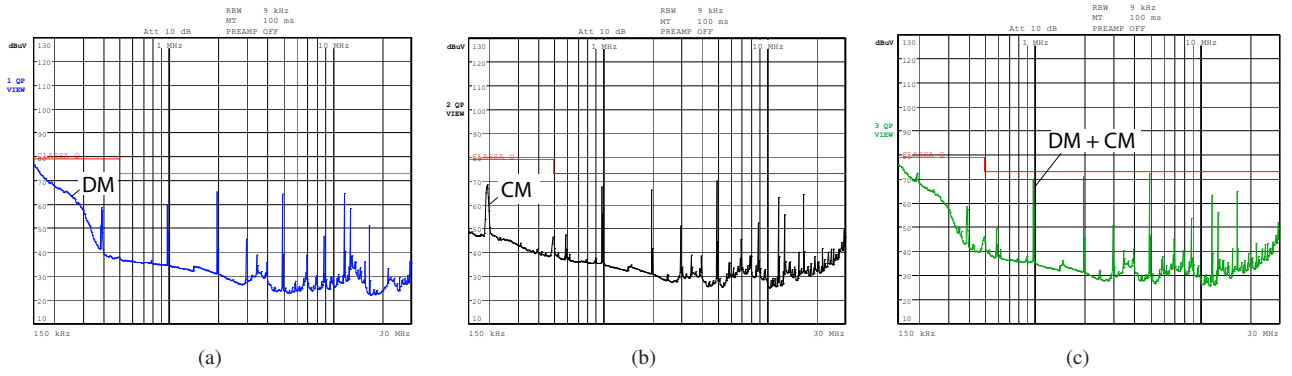
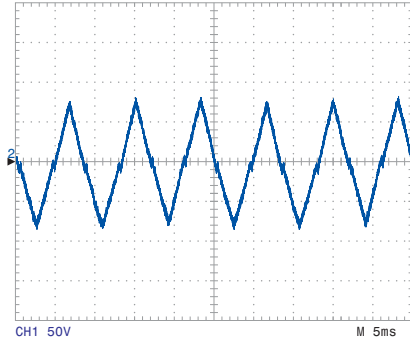
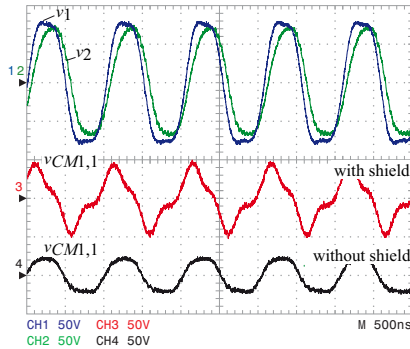


Fig. 11: Final CE measurements of the realized rectifier system; (a) DM emissions, (b) CM emissions and (c) total conducted emissions.



(a)



(b)

Fig. 12: (a) Measured CM output voltage component form (from M to earth) employing the proposed CM filter concept and (b) measured voltage of CM inductor $L_{CM1,1}$ with and without PCB shield layer connected to M .

separator was applied to measure the DM and CM noise separately [22]. As expected, the main peaks in the spectra occur at f_s and $2f_s$ and are well below the limit. The peak at 5 MHz results from a shielding layer in the printed circuit board and will be discussed later. The peak in the DM spectrum at 400 kHz has its source in the auxiliary power supply and the peak of the CM emissions at 200 kHz is caused by the auxiliary supplies of the gate drives.

Fig. 12(a) shows the voltage of the output midpoint against earth. No high-frequency CM voltage is present and only the third harmonic triangular signal $v_{CM,h3}$, used for increasing the rectifier modulation range is measured. This verifies the proper operation of the proposed CM filter concept. Deviations from the triangle signal can be observed at the zero-crossings. There, the CM chokes are able to hold the total CM voltage v_{CM} without saturation and the voltage stays zero. After reaching light saturation C_{FB} is charged and the system operates as intended.

As can be seen in Fig. 10(a), the DM inductors C_{DM1} and C_{DM2} are arranged face to face and are therefore magnetically coupled. This parasitic effect reduces the attenuation of the DM

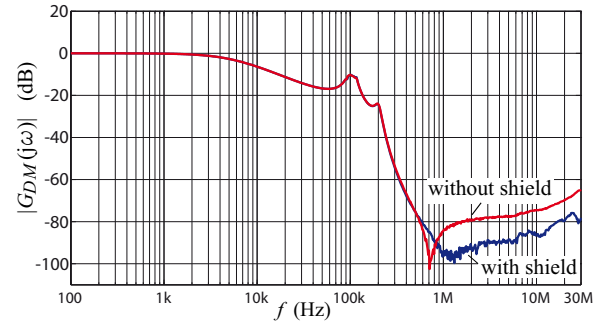


Fig. 13: Measured transfer function $G(j\omega)$ of the DM filter with and without shield.

filter stage and hence a magnetic shield (0.1 mm thick Mu-metal foil glued on a PCB with solid copper layer) is inserted between the two stages to reduce the coupling (also shown in Fig. 10(a)). In Fig. 13 the measured transfer function $G_{DM}(j\omega)$ of the filter with and without the shield is plotted. Whereas for frequencies below 800 kHz no difference occurs, an improvement of ≈ 10 dB can be measured for frequencies above 1 MHz. It has to be stated here that the dynamic range of the used network analyzer Bode100 [23] is 100 dB and that the measurement results are therefore limited to this value.

Next, the influence of the arrangement of the first DM and CM filter stages (impedance mismatch) is examined. For this purpose, the DM filter capacitors C_{DM2} are moved behind the CM choke L_{CM2} (cf., Fig. 14(a)). As nothing is changed for the CM path the three Y2-capacitors (4.7 nF) now constitute an additional DM filter stage with the leakage inductance of the CM choke. Unfortunately, the impedance of the Y2-capacitors $|Z_{C,CM2}|_{1\text{MHz}} = 1/\omega C_{CM2} = 33.8 \Omega$ is in the same range as the DM impedance of the LISN ($R_{LISN,DM} = 50 \Omega$) and therefore doesn't fulfill the impedance mismatch criteria. This results in 10 dB higher noise level compared to a realization satisfying the impedance mismatch criteria (cf., Fig. 14(b)). Therefore, the arrangement of filter stages has to be handled with care in order to achieve the desired attenuation.

In the following the question if a solid copper layer in the printed circuit board (PCB) covering the whole power and EMI arrangement could act as an advantageous shielding layer is discussed. There, the intention is to connect this copper layer to M in order to catch high-frequency noise currents similar to the proposed CM filter concept. Unfortunately, this shield layer also introduces a (capacitive) coupling path from the interconnections of the three CM chokes forming L_{CM1} to M (cf., Fig. 9). Because of these capacitive couplings, a uniform voltage distribution between the three CM chokes is inhibited. According to the measurement given in Fig. 12(b) a phase-shift of the voltage

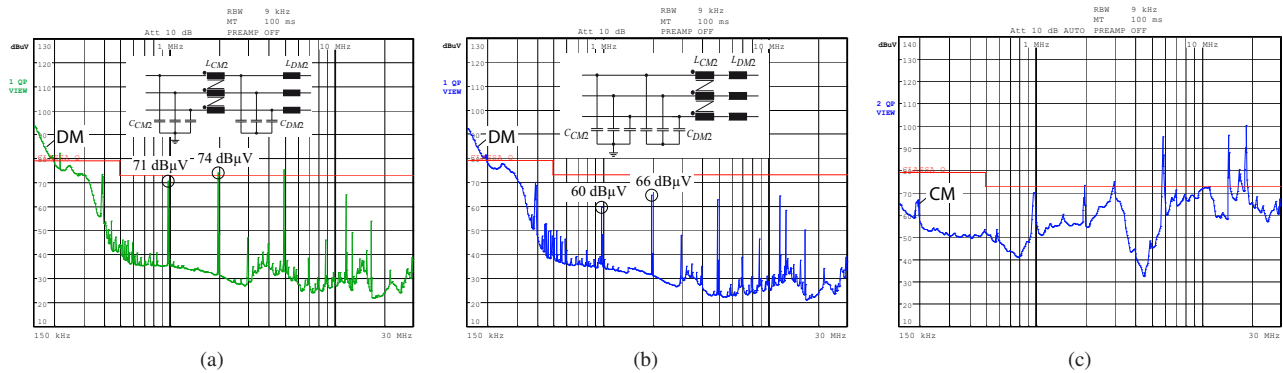


Fig. 14: (a) Measured DM emissions if the CM filter stage arrangement violates the impedance mismatch criteria for the DM filter stage and (b) measured DM emissions if filter satisfies the impedance mismatch criteria. Measured CM emissions with unfavorable copper shielding layer in the printed circuit board. The CM filter is short circuited by the shielding layer for frequencies above 5 MHz.

v_2 (after the first CM inductor $L_{CM1,1}$) drives this inductor into saturation ($v_{CM1,1}$ with shield). However, if the shielding layer is not connected to M a uniform voltage distribution occurs which can be verified by the measured voltage ($v_{CM1,1}$ without shield) which amplitude corresponds to $v_{CM, \sim}/3$.

If the shielding layer is left open, another effect can be observed: The copper layer covers the whole EMI filter and causes a capacitive coupling which forms a low-impedance path short circuiting the EMI filter at higher frequencies. An EMI measurement only considering CM emissions with a copper layer beneath the whole EMI filter is given in Fig. 14(c) and verifies increased emissions. For the final realization this copper layer was cut after the CM inductors L_{CM1} but the remaining part still causes a noise peak at 5 MHz in Fig. 11. Hence, shielding layers have to be handled with special care in order not to degrade the filter performance.

VI. CONCLUSION

This paper presented the design of an EMI filter for an ultra-compact 10 kW three-phase/level PWM rectifier. Filter requirements have been derived using computer simulations. A specific CM filter strategy has been proposed, where the output of the rectifier shows no high-frequency CM voltage. The performance of the novel filter concept has been analyzed and the CM inductor L_{CM} turned out to be the key element for a successful implementation of the proposed concept. For a better understanding of CM behavior an extended CM model of the rectifier system has been derived which demonstrated also the occurrence of “mixed-mode emissions”. A 10 kW laboratory prototype with a power density of 14.1 kW/dm³ and a switching frequency of 1 MHz has been realized. The performance of the designed EMI filter has been verified by measurements taken from this prototype. Modifications on several filter parts have shown that a careful component selection as well as a proper arrangement and layout is essential for achieving a satisfactory EMI filter performance.

REFERENCES

- [1] J.A. Rosero, J.A. Ortega, E. Aldabas, and L. Romeral, “Moving towards a more electric aircraft,” *IEEE Magazine on Aerospace and Electronic Systems*, Vol.22, No.3, March 2007, pp.3-9.
- [2] R.W. Erickson, and D. Maksimovic, “Fundamentals of Power Electronics (2nd ed.),” *Springer Science+Business Media, LLC*, 2001.
- [3] A. Nagel, and R.W. De Doncker, “Systematic design of EMI-filters for power converters,” *Proc. of the IEEE IAS 2000*, Oct 2000, Vol.4, pp.2523-2525.
- [4] S. Qu, and D. Chen, “Mixed-mode EMI noise and its implications to filter design in offline switching power supplies,” *IEEE Trans. Power Electron.* Vol.17, No.4, Jul 2002, pp.502-507.
- [5] J. Meng, and M. Weiming, “A new technique for modeling and analysis of mixed-mode conducted EMI noise,” *IEEE Trans. Power Electron.*, Vol.19, No.6, Nov. 2004, pp. 1679-1687.
- [6] W. Shen, F. Wang, and D. Boroyevich, “Conducted EMI characteristic and its implications to filter design in 3-phase diode front-end converters,” *Proc. of the IAS 2004*, Vol.3, 3-7 Oct. 2004, pp. 1840-1846.
- [7] W. Shen, F. Wang, D. Boroyevich, and Y. Liu, “Definition and acquisition of CM and DM EMI noise for general-purpose adjustable speed motor drives,” *Proc. of the PESC’04*, Vol.2, 20-25 June 2004, pp. 1028-1033.
- [8] T. Nussbaumer, M.L. Heldwein, and J.W. Kolar, “Differential Mode Input Filter Design for a Three-Phase Buck-Type PWM Rectifier Based on Modeling of the EMC Test Receiver,” *IEEE Trans. Ind. Electron.*, Vol.53, No.5, Oct. 2006, pp.1649-1661.
- [9] G. Laimer, and J.W. Kolar, “Zero-ripple EMI input filter concepts for application in a 1-U 500 kHz Si/SiC three-phase PWM rectifier,” *Proc. of the INTELEC’03*, 19-23 Oct. 2003, pp. 750-756.
- [10] Yifan Zhao, Yue Li, and T.A. Lipo, “Force commutated three level boost type rectifier,” *IEEE Trans. Ind. Appl.*, Vol.31, No.1, Jan/Feb 1995, pp.155-161.
- [11] M.L. Heldwein, and J. W. Kolar, “Impact of EMC Filters on the Power Density of Modern Three-Phase PWM Converters,” *IEEE Trans. Power Electron.*, Vol.24, No.6, June 2009, pp.1577-1588.
- [12] J.W. Kolar, U. Drogenik, J. Minibock, and H. Ertl, “A new concept for minimizing high-frequency common-mode EMI of three-phase PWM rectifier systems keeping high utilization of the output voltage,” *Proc. of the APEC 2000*, Vol.1, pp.519-527.
- [13] H. Joergensen, S. Guttowski, and K. Heumann, “Comparison of Methods to Reduce the Common Mode Noise Emission of PWM Voltage-Fed Inverters,” *Proc. of the 37th Int. Power Conf. Conf.*, Nuremberg, Germany, May 26-28 1998, pp. 273-280.
- [14] IEC International Special Committee on Ratio Interference - C.I.S.P.R.(2004), “Specification for Industrial, scientific and medical (ISM) radio-frequency equipment - Electromagnetic disturbance characteristics - Limits and methods of measurement - Publication 11,” Geneva, Switzerland.
- [15] K. Raggl, T. Nussbaumer, and J.W. Kolar, “Guideline for a Simplified Differential Mode EMI Filter Design,” Accepted for future publication in the *IEEE Trans. Ind. Electron.* (2009).
- [16] D.G. Holmes, “A general analytical method for determining the theoretical harmonic components of carrier based PWM strategies,” *Proc. of the 33rd IAS Industry Appl. Conf.*, vol.2, 12-15 Oct 1998, pp.1207-1214.
- [17] H. Deng, L. Helle, Yin Bo, and K.B. Larsen, “A General Solution for Theoretical Harmonic Components of Carrier Based PWM Schemes,” *Proc. of the APEC 2009*, 15-19 Feb. 2009, pp.1698-1703.
- [18] M.L. Heldwein, and J.W. Kolar, “Design of Minimum Volume Input Filters for an Ultra Compact Three-Phase PWM Rectifier,” *Proc. of the 9th Brazilian Power Electron. Conf. (COBEP’07)*, 2007, Vol.1, pp.454-461.
- [19] H. Ye et al., “Common mode noise modeling and analysis of dual boost PFC circuit,” *Proc. of the INTELEC 2004*, 19-23 Sept. 2004, pp. 575-582.
- [20] S. Wang, P. Kong, and F.C. Lee, “Common Mode Noise Reduction for Boost Converters Using General Balance Technique,” *IEEE Trans. Power Electron.*, Vol.22, No.4, July 2007
- [21] S. Shuo Wang; F.C. Lee, W.G. Odendaal, “Improving the performance of boost PFC EMI filters,” *Proc of the APEC ’03*, 9-13 Feb. 2003, Vol.1, pp. 368-374.
- [22] M.L. Heldwein, T. Nussbaumer, F. Beck, and J.W. Kolar, “Novel three-phase CM/DM conducted emissions separator,” *Proc. of the APEC ’05*, Vol.2, 6-10 March 2005, pp.797-802.
- [23] Omicron electronics. (2008). Handbook of the network vector analyzer: Bode100 [Online]. Available: www.omicron-labs.com
- [24] IEC International Special Committee on Ratio Interference - C.I.S.P.R.(1977), “C.I.S.P.R. Specification for Radio Interference Measuring Apparatus and Measurement Methods - Publication 16,” Geneva, Switzerland.